UCID- 20263

EXPERIMENTS ON ETA COMPARING WIRE-CONDITIONED AND NON-WIRE-CONDITIONED BEAM PROPAGATION

J. C. Clark
E. J. Lauer
D. S. Prono
K. W. Struve

January 18, 1984

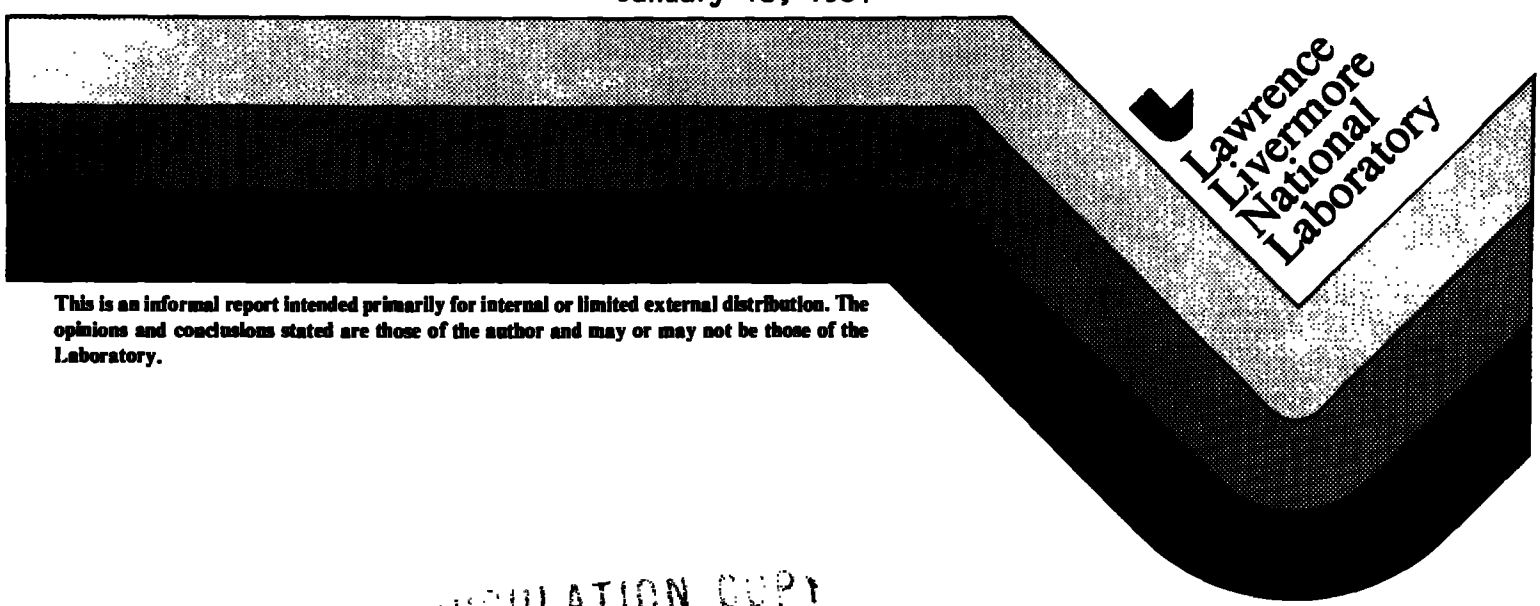

Printed in the United States of America
Available from
National Technical Information Service
U.S. Department of Commerce
5285 Port Royal Road
Springfield, VA 22161
Price: Printed Copy $; Microfiche $4.50

Page Range	Domestic Price	Page Range	Domestic Price
001-025	$ 7.00	326-350	$ 26.50
026-050	8.50	351-375	28.00
051-075	10.00	376-400	29.50
076-100	11.50	401-426	31.00
101-125	13.00	427-450	32.50
126-150	14.50	451-475	34.00
151-175	16.00	476-500	35.50
176-200	17.50	501-525	37.00
201-225	19.00	526-550	38.50
226-250	20.50	551-575	40.00
251-275	22.00	576-600	41.50
276-300	23.50	601-up[1]	
301-325	25.00		

[1]Add 1.50 for each additional 25 page increment, or portion thereof from 601 pages up.

EXPERIMENTS ON ETA COMPARING WIRE-CONDITIONED AND NON-WIRE-CONDITIONED BEAM PROPAGATION

J. C. Clark, E. J. Lauer, D. S. Prono, K. W. Struve

January 18, 1984

Lawrence Livermore National Laboratory
University of California
Livermore, California 94550

ABSTRACT

This report describes experiments in beam propagation with the ETA beam during 1982 following accelerator cavity modifications which allowed a maximum beam current of up to 8 kA at the entrance to the propagation tank. A prominent new feature of the propagation in high pressure gas was an enhancement of the net current as the beam propagated. In some cases this enhanced current was nearly double the injected beam current. The strong current enhancement was associated with strong transverse hose motion of the beam. The absence of microwave emissions in the range from 6.6 GHz to 31 GHz indicates that this current enhancement is not due to a two-stream instability.

Work performed jointly under the auspices of the U. S. Department of Energy by Lawrence Livermore National Laboratory under contract W-7405-ENG-48 and for the Department of Defense under Defense Advanced Research Projects Agency ARPA Order No. 4395 Amendment No. 31, monitored by Naval Surface Weapons Center under document number N60921-84-WR-W0080.

A wire zone was later added in the transport region between the accelerator and the propagation tank to further damp the BBU instability and, also, reduce the lower frequency sweep oscillations on the beam. This modification increased the beam size and reduced the peak current at the entrance to the propagation tank to 4.5 kA. Additional propagation measurements with this beam in a longer tank showed some improvement in propagation with reduced hose growth and less current enhancement.

At very short propagation lengths, too short for the hose instability to grow, there is a current enhancement at pressures greater than 200 torr that can be explained by fast secondary electrons pushed forward by the beam self-magnetic field.

I. INTRODUCTION

This report describes propagation experiments with the ETA beam that were conducted during 1982. Several modifications to the accelerator were made since the last reported propagation studies [Ref. 1]. These changes have greatly improved the beam characteristics from the accelerator. In particular, the accelerator cavities were modified to reduce the growth rate of the beam break-up (BBU) instability [Ref. 2]. This modification allowed beam currents of up to 8 kA at the entrance to the propagation tank as compared to 4.5 kA achieved in previous experiments. However, the beam continued to exhibit a low frequency transverse sweep with frequency and amplitude somewhat dependent on tuning of focusing and steering magnets. Typically the sweep was seen to

have frequency components in the 100 to 500 MHz range, with displacements of 1 to 2 cm. Experiments with a 1.5 m long carbon filament wire, installed along the center of a section of the transport pipe between the accelerator and the propagation tank, showed that both high and low frequency transverse motions of the beam could be significantly damped [Ref. 3].

Results from two different experimental configurations are described. The first set of experiments were done with a 65 cm long propagation tank containing either air, nitrogen or neon without a carbon wire to condition the beam. A prominent feature of this propagation was an enhancement of the net current in gas as the beam propagated. In some cases this enhanced current became nearly double the injected beam current.

In the second configuration, a wire-conditioned beam was propagated in a 5.3 m long experimental cell. The most obvious effect of the wire zone, besides damping the transverse motion, was to increase the beam radius by a factor of 4 to 5 and to decrease the peak current to 4.5 kA at the entrance to the experimental cell. These experiments were done in neon to simulate the effects of conductivity growth to be expected from the higher energy 10 kA ATA beam propagating in air. Some current enhancement was observed at a longer propagation distance. The beam, also, propagated much further without being grossly disrupted by the hose instability. However, when scaled to an on-axis betatron wavelength, the effective propagation distance was less than twice as long as that for the unconditioned beam in the short cell.

II. EXPERIMENTAL DESCRIPTION

The short propagation cell is shown in Fig. 1. It consisted of a 65 cm section of metal pipe similar to the beam transport from the accelerator. The propagation cell could be filled with gas at various pressures and was separated from the vacuum section of the accelerator by a 0.030 mm thick titanium foil. This foil was located between a pair of current monitors labeled #9 and #10 in Fig. 1. The first monitor measured the current from the accelerator on the vacuum side of the foil. The second measured the net current, the algebraic sum of the beam current and the return current in the gas, on the gas side. The current monitors #11 and #12 measured the net current at their respective positions of 40 cm and 65 cm from the entry foil. Between current monitors #12 and #13, there was a second titanium foil with a 6 cm aperture. Current monitor #13 was in vacuum; it measured the beam current that propagated through the gas. Current monitor #14 was added for some of the experiments. It was in vacuum and had a 3 cm diameter aperture.

The long propagation cell for the experiments with a wire-conditioned beam is shown in Fig. 2. The basic cell consists of sections of 14.6 cm ID aluminum tubing with current monitors as shown. In this case, the entry foil had a 6 cm diameter aperture as in the previous short experimental cell; however, the foil at 5.3 m between current monitors #13 and #14 was the full diameter of the experimental tank. Monitor #15 in vacuum had a 6 cm aperture.

III. BEAM PROPAGATION DIAGNOSTICS

The principal diagnostic tool for these propagation experiments was the current monitors [Ref. 4]. In addition, a fast-gated TV system was used to look at the entry foil through a port located on an angle of 30° to the beam line. Another TV was used to look at the beam light through the side ports in the first 30 cm of the experimental cell.

Microwave emissions from the beam-produced plasma were picked up with two X-band waveguides mounted flush with the propagation tank wall 30 cm downstream from the entry foil. The experimental arrangement is shown in Fig. 3. The ends of the waveguide served as wide acceptance angle antennas and were oriented so that the waveguide E-plane was parallel to the propagation direction. The waveguides also acted as high pass filters, having a low frequency cut-off at 6.6 GHz. Both lines were brought through the shield and terminated roughly 4 m from the propagation tank. The first line included a 16 GHz low pass filter, resulting in a 6.6 to 16 GHz bandpass. The second line transitioned to a K-band waveguide, which has a low frequency cut-off at 14.1 GHz. It also had a 31 GHz low pass filter, resulting in a 14.1 to 31 GHz bandpass.

Broadband crystal detectors were mounted at the end of each waveguide. Their output voltage was proportional to the input microwave power. However, the attenuation of the two waveguide lines was not measured, and the gain of the waveguide antennas, which depends on both the frequency of emissions and on the location of the emitting plasma, was not determined. Approximate values of the power level can be estimated from the CW detector calibrations; 2.5 mW/volt for the 6.6 to 16 GHz detector, and 3.3 mW/volt for the 14.1 to 31 GHz detector. We stress that the most important information is the pressure dependence of the output, which is calibration independent.

Later in the experimental program, some beam diameter measurements were made using a wire of high Z material (Ta, W) which scanned through the beam. The x-rays generated were detected by a fast fluor and a photomultiplier tube. Thus, a profile of the beam is obtained from an Abel inversion of the x-ray signal as a function of wire position.

The propagation experiments were made by filling the cell to the desired pressure from a compressed gas bottle through an externally controlled leak valve. The pressure was monitored with a Baratron pressure gauge that can measure in the range from 1 m torr to 1000 torr. The pressure range of gases used was 80 m torr to 500 torr in air (wet and dry), nitrogen and neon. The gas pressure was typically varied in a 1, 2, 5, 10 decade pressure sequence.

IV. EXPERIMENTAL RESULTS

Short Cell, Non-Wire-Conditioned Beam

The initial beam conditions for these experiments was usually a 4.2 MeV beam energy with 7.5 kA of peak current in a 25 ns FWHM pulse. A typical current pulse is shown in Fig. 4. The beam radius varied from 0.35 to 0.5 cm HWHM, as measured from the entry foil light with the gated TV and with the x-ray wire scans.

Air, Nitrogen

The peak current recorded at each current monitor in the gas was plotted as a function of pressure. The most prominent feature of the gas propagation in this experimental configuration is an enhancement of the net current as the beam propagates in the gas. Typical curves of this peak current as a function

of pressure for air and nitrogen are shown in Fig. 5. At 40 cm from the entry foil the net current becomes greater than the injected beam current as the pressure is increased above 20 torr. After the beam has propagated 65 cm the point at which the net current exceeds the injected current occurs at 10 torr. At pressures above 100 torr the enhancement begins to dissipate as the beam edge hits the walls of the test cell. The current enhancement shown at pressures of a few tenths of a torr has been previously explained as due to a two-stream instability [Ref. 5]. There was no distinguishable difference in these current characteristics between air and nitrogen.

Current enhancement of the order of 10% above the injected current was detected even at very short propagation lengths. This is shown in Fig. 5(a) and more directly in Fig. 6 which shows some typical current monitor traces. The injected current is shown in the vacuum traces, but as the pressure is increased the net current is clearly greater than the injected beam current at 200 and 500 torr. This effect is likely due to energetic secondary electrons (delta rays) that are pushed forward by the beam self-magnetic field [Ref. 6].

The current enhancement away from the entry foil is a strong function of current density as is shown in Fig. 7. For these results, the peak beam current at the entry foil was 6.5 kA. The beam diameter was set to 0.7 cm FWHM as measured with the entry foil TV, and a pressure scan from 20 to 200 torr in nitrogen was taken. The focus of the final magnetic lens was then relaxed so that the beam diameter expanded to 0.9 cm FWHM while maintaining the same total current, and the pressure scan was repeated. The peak net current after propagation of 40 cm is dramatically reduced for the lower current density.

The current enhancement also is a function of the distance propagated. This effect is seen by comparing net currents after 65 cm of propagation as shown in Fig. 8 with those after 40 cm of propagation as shown in Fig. 7. After additional propagation length, the hose instability grows to the point that the beam breaks up; the current enhancement peaks and finally dissipates with distance. A typical set of the time histories at each of the current monitors at a fixed pressure is shown in Fig. 9. For this case there is very strong current enhancement at 40 cm from the entrance foil. The initial rise of the net current is similar to that of the beam current; however, as the net current reaches nearly the peak beam current, there is a very sudden rise to nearly twice the peak beam current. The onset of this sudden rise in peak current is not pressure dependent; only its peak value is. At 65 cm from the entry foil, the net current is unstable in amplitude and appears to have partially terminated on the tank wall.

The beam charge transported through to current monitor #13 is shown in Fig. 10. The total charge transported is a better measure of beam transport than is peak current when the latter is influenced by narrow spikes of current which occur as the beam hoses strongly at higher pressures.

With this measure the optimum propagation pressure was between 2 and 5 torr. This is the expected region of good propagation based on the previous FX-25 experiments [Ref. 7].

Some experiments at the higher pressures were also done with wet air. Beam propagation was not perceptively distinguishable from that in dry air, though the optical emission spectra were drastically different [Ref. 8]. The wet air runs showed similar current enhancement.

Neon

Similar current enhancement propagation effects were seen in neon. Figure 11 shows the peak net currents in the gas at entry, 40 cm, and 65 cm, and the peak beam current at 65 cm for both an 8 kA and a 4 kA beam. Also shown are some corresponding predictions by the EMPULSE code of the net current expected in neon for the pressure range from 10 to 100 torr. The code results compare favorably with the measured net currents.

A representative set of the current monitor time traces at 100 torr Neon is shown in Fig. 12. When the current enhancement occurs at some distance from the entrance foil it is accompanied by a strong transverse displacement of the beam as shown by the x and y traces at current monitor #11. The current enhancement is still very strong at 65 cm, though the amplitude is more variable pulse-to-pulse. Here, the transverse motion is even larger than at 40 cm. (Note the scale change on the x, y traces.) The beam charge transported through 65 cm of neon as a function of pressure is shown in Fig. 13. The region of good propagation is 5 to 10 torr, again, as expected from FX-25 experiments.

Microwave Emissions

Microwave emissions were monitored as a function of air pressure in the propagation tank. The wire zone was not used during these measurements. (When the wire was in place, microwave emissions were reduced roughly three orders of magnitude, making them barely detectable). Data from a typical pressure scan are shown in Fig. 14 where peak microwave power detected in the 6.6 to 16 GHz and the 14.1 to 31 GHz frequency bands is plotted as a function of gas tank pressure. The vertical scale is the detector output in volts, which is proportional to the input microwave power. The signal in both bands

rises abruptly between 40 and 80 microns pressure and peaks around 100 to 200 microns. At higher pressures, the microwave power falls until at 3 torr it is a thousand times lower. At higher pressures the microwave signal was not detectable above the noise. The points above 3 torr thus represent the minimum detectable signal. These measurements were repeated on several different runs. Generally, the shape of the curves stayed the same, with the peak amplitude and the pressure of the peak amplitude varying slightly. The amplitude could vary as much as 50 percent from shot to shot. At low pressures, the microwave emission results from the two-stream instability between the beam and plasma electrons [Ref. 5]. This two-stream interaction with a relativistic beam is accompanied by strong current enhancement. As the beam enters the gas, it ionizes a plasma channel. The resulting plasma electrons are ejected by the radial electric field of the beam and can reach the metallic wall when the neutral gas density is low enough that collisions with the neutrals do not occur. The ions are more immobile and remain in the channel. For sufficiently high neutral gas pressures, the ion density can equal or exceed the beam electron density. In that case, not all electrons are ejected from the region of the beam, and a two-stream instability results. As the neutral pressure is raised, the electron-neutral collision frequency increases. At pressures above approximately 5 torr, it is sufficiently high to stabilize the two-stream instability [Ref. 9].

The absence of microwave emissions above 10 torr indicates that a two-stream instability is not contributing to the observed current enhancement at the higher pressures. Simultaneous measurements of the net current and the microwave emission show current enhancement without a corresponding microwave signal.

V. LONG CELL WIRE-CONDITIONED BEAM

The best technique currently available to reduce the beam sweep and concomitantly to reduce any BBU oscillations is to use a wire zone transport. The characteristics of the resulting beam at the entry point (monitor #10) of the evacuated propagation cell were: 1) beam energy 4.2 MeV, 2) peak beam current of 4.5 kA in a 25 ns FWHM beam, 3) beam radius of 2.2 cm HWHM. Note that the beam is so large that there is some loss of current between monitor #9 and #10 on the 6 cm diameter aperture at the entry foil.

Air

A few measurements were taken in the long cell with air and nitrogen gas at pressures above 1 torr. A 10 to 15 percent current enhancement was observed at 50 and 100 torr of nitrogen 40 cm from the entry foil.

Neon

A series of propagation experiments were done in neon gas. Figure 15(a) shows the peak net current at the entry foil as a function of pressure. In this case there is less than 50 percent current neutralization with the maximum neutralization occurring at 2 torr. After 40 cm of propagation, the net current is changed very little as shown in Fig. 15(b), though there is a trend to slightly increased net currents at the higher pressures, possibly showing incipient current enhancement. After propagation of 2.7 meters, significant current enhancement is evident at 20 torr as shown in Fig. 15(c). As the pressure is increased, a growing hose instability has caused some of the beam to hit the wall, reducing the detected net current. The hose instability disrupts the tail of the pulse at the lower pressures and moves forward in the pulse as the pressure is increased. No current enhancement is noted at

5.3 meters of propagation. Above 200 torr, the beam is stabilized against hose motion, but is very broad with a low current density. This is consistent with a calculated Nordsieck scattering length at 200 torr of approximately 3 meters. Finally, as shown in Fig. 15(d), after 5.3 m of propagation, detectable net currents exist only at pressures less than 100 torr. The peak beam current and the beam charge transported the full 5.3 meters through neon, as measured by a vacuum current monitor, is shown in Figs. 16 and 17 respectively. Good propagation is observed at 5 torr, as was found in FX-25 experiments.

Comparison Of Wire-Conditioned Beam With Non-Wire-Conditioned Beam

Quantitative comparison of propagation for the wire-conditioned and non-wire-conditioned beam must be made in terms of an appropriate scale length that characterizes beam propagation. The on-axis betatron wavelength depends on the net current density on axis. The net current measured by the wall current monitors only gives an indication of $J_{NET}(r = 0)$. To compute the actual on-axis betatron wavelength or a mean betatron wavelength for the entire radial distribution of current, requires a detailed knowledge of $J_B(r)$ and $J_{NET}(r)$ for each case. Moreover, the net current as measured is z dependent and varies widely, especially where current multiplication is strong. Hence, for a first parameterization of the two experiments we use the beam current to compute the on-axis unneutralized betatron wavelength. We note that the current enters into the calculation only as a square root.

The typical beam current at injection for the non-wire-conditioned beam was 7.5 kA. The beam size at entry was measured with the gated TV to be between 0.35 and 0.5 cm. A measurement using the x-ray wire at 16 cm behind the entry foil in 80 m torr of nitrogen showed R_{HWHM} to be 0.44 cm. For the

non-wire-conditioned beam we assume a Bennett distribution and a beam radius of $R_{HWHM} = 0.45$ cm. The on-axis current density is given by

$$J_{BO} = \frac{I_B}{\pi R_B^2} \quad .$$

The R_{HWHM} in terms of the Bennett radius R_B is obtained from

$$\frac{J_{BO}}{2} = \frac{J_{BO}}{\left(1 + \frac{R_{HWHM}^2}{R_B^2}\right)^2}$$

or $$R_{HWHM} = 0.64\ R_B \quad .$$

Then,

$$\lambda_{\beta O} = 2\pi R_B \left(\frac{I_A}{2I_B}\right)^{1/2}$$

$$= 14.3 \text{ cm} \quad .$$

Thus there are 4.5 betatron wavelengths in the 65 cm cell for this comparison.

The wire-conditioned beam at the entry to the propagation cell was apertured by the entry foil holder of 6 cm diameter. The outer edge of the beam was stripped off by this aperture, and the entry foil TV could not give a measure of beam radius in this case. An x-ray scan at 2.8 meters showed the equilibrium radius at 80 mtorr to be $R_{HWHM} = 2.2$ cm. The typical current injected into the cell was 4.5 kA. Thus,

$$\lambda_{\beta O} = \frac{2\pi R_{HWHM}}{0.64} \left(\frac{I_A}{2I_B}\right)^{1/2} = 94 \text{ cm} \quad .$$

This predicts 5.9 betatron wavelengths in the 5.3 m cell for the non-wire-conditioned beam. By this comparison the long tank had only 1.3 times as many on-axis betatron wavelengths.

In the pressure region where the beam propagates well (1 - 2 torr air and 5 - 10 torr neon), the net current was nearly the same for both the wire-conditioned and non-wire-conditioned beam, independent of the initial beam current. A calculation of the betatron wavelength for this region using a net current of 2 kA for both cases, shows the short tank to be 2.35 betatron wavelengths long and the long tank to be 3.91 betatron wavelengths long, or 1.7 times as many betatron wavelengths.

Nose Erosion

In the pressure regions where the beam was able to propagate well, it was possible to measure the nose propagation speed of the beam using the beam current monitors with careful measurement of the timing. For beam propagation in air, these measurements are shown in Figs. 18(a), (b), and (c) for pressures of 0.08, 1 and 10 torr respectively. Each figure shows the propagation time for the initial rise of current at 100 amps and also at 1 kA. At 0.08 torr there is first an early blow-off of the nose in the first 40 cm and then a steady erosion rate of 0.18. At 1 and 10 torr, the beam has an initial blow-off that is complicated by the pinching of the beam in the first 40 cm of propagation. This combination gives the beam the appearance of propagating faster than c at the 1 kA level. Thereafter, the beam propagates with very little nose erosion.

These effects for propagation in neon at 0.08 torr and 5 torr are shown in Figs. 19(a) and (b). There is an even more pronounced blow-off in neon at 0.08 torr and a faster erosion rate of 0.30. At 5 torr, there is also a large initial blow-off and, thereafter, subsequent propagation with very little erosion.

VI. SUMMARY AND DISCUSSION

The most notable new feature observed in these experiments is current enhancement ($I_{net} > I_{beam}$) at high pressures in the range of 10 to 500 torr. The effect is distinctly different than that observed at low pressures (less than 1 torr), which has been identified as due to two-stream instability. In this high pressure case, there is no microwave emission in the bands from 6.6 GHz to 31 GHz.

A theory has been proposed to explain current enhancement as energetic secondary electrons pushed forward by the beam self-magnetic field [Ref. 6]. This model can account for current enhancement of up to 15 percent above the injected beam current; however, measurements have shown as much as 90 percent enhancement. The current enhancement measured at high pressure and a short propagation length are consistent with this model. However, the current enhancement which grows with propagation length and is related to hose motion cannot be explained by these delta currents.

The experiments with the wire-conditioned beam gave some indication of improved propagation with reduced hose growth and less current enhancement. Scaled to betatron wavelength, the long tank was about 1.7 times longer for the region of good propagation, and 1.3 times longer at higher pressures where the net current is equal to the injected beam current. The beam was so large that the Nordsieck scattering limited useful propagation measurements at higher pressures. Further experiments with a wire-conditioned beam would be of interest if the diameter could be reduced to allow a propagation length greater than 10 $\lambda_{\beta 0}$.

Further efforts to measure the energy content of the forward current outside the primary beam and further efforts to measure the radial extent of the beam in the region of maximum current enhancement would be helpful to identify the mechanism responsible for current enhancement.

FIGURES

Figure 1. Short propagation cell used for studies of non-wire-conditioned beam.

Figure 2. Long propagation cell used for wire-conditioned beam studies.

Figure 3. Configuration of the microwave emissions measurements. a) Cross-section of the propagation tank at the microwave port, b) Schematic of the detection technique.

Figure 4. Typical current pulse at entry to the beam propagation cell. (a) Current (b) Position.

Figure 5. Peak net currents in air or nitrogen as a function of pressure from 80 m torr to 500 torr at: (a) Entry foil in gas, (b) 40 cm in gas and (c) 65 cm in gas.

Figure 6. Beam current oscilloscope traces for the beam at the entrance to the experimental cell. Current monitor #9 shows the current in vacuum just in front of the entrance foil. Monitor #10 shows the net current just after the foil in vacuum (beam current), and at 200 torr and 500 torr in air.

Figure 7. Peak net current vs pressure for beam in air for two different beam sizes, 0.7 cm FWHM and 0.9 cm FWHM at 40 cm from entrance foil.

Figure 8. Peak net current vs pressure for beam in air at 65 cm from entrance foil.

Figure 9. Typical oscilloscope time traces for each current monitor in 50 torr air. (4 pulses overlaid)

Figure 10. Beam charge transported through 65 cm of air as a function of the pressure of air in the propagation cell.

Figure 11. Peak net current in neon as a function of pressure from 80 m torr to 500 torr at: (a) Entry in gas, (b) 40 cm in gas, (c) 65 cm in gas, and (d) peak beam current propagating through 65 cm of neon.

Figure 12. Typical oscilloscope time traces for the current monitors in 100 torr neon. (4 pulses overlaid)

Figure 13. Beam charge transported through 65 cm of neon as a function of the pressure of neon in the propagation cell.

Figure 14. Microwave emission from the beam-produced plasma as a function of pressure. The vertical scale is the detector output in volts and is proportional to the microwave power.

Figure 15. Peak net current vs pressure for a wire-conditioned beam in neon as a function of pressure at: (a) entry foil, (b) 40 cm in gas, (c) 2.7 m in gas, (d) 5.3 m in gas.

Figure 16. Peak beam current propagated through 5.3 cm of neon as a function of pressure for a wire-conditioned beam.

Figure 17. Beam charge propagated through 5.3 m of neon as a function of pressure for a wire-conditioned beam.

Figure 18. Beam head propagation time at 100 A and at 1 kA for 5.3 m of propagation in air at: (a) 80 m torr, (b) 1 torr, and (c) 10 torr, showing beam head erosion.

Figure 19. Beam head propagation time at 100 A and at 1 kA for 5.3 m of propagation in neon at (a) 80 m torr and (b) 5 torr, showing beam head erosion.

REFERENCES

1. F. W. Chambers, J. C. Clark and T. J. Fessenden, "Comparison of the Initial ETA Gas Propagation Experiments," UCID-19383, LLNL, April 20, 1983.

2. G. J. Caporaso, A. G. Cole, K. W. Struve, "Beam Breakup (BBU) Instability Experiments on ETA, and Predictions for ATA." IEEE on Nuc. Sci Vol. NS-30, vol. 4, Part I of Two, pp. 2507.

3. D. S. Prono, G. J. Caporaso, J. C. Clark, E. J. Lauer and K. W. Struve, "A Simple Method for Damping Transverse Motion of a High Intensity Electron Beam," IEEE Trans. on Nuc. Sci, Vol. NS-30, No. 4, Part I of Two, pp. 2510.

4. These monitors have evolved from similar monitors used on the Astron accelerator and described by Fessenden, Stallard, and Berg, in RSI 43 1789, (1972).

5. F. W. Chambers, "Current Multiplication During Relativistic E-beam Propagation in Plasma," Physics of Fluids, Vol. 22, No. 3, pp. 483, March 1979.

6. S. S. Yu and R. E. Melendez, "Model of Current Enhancement at High Pressure," UCID-19965, LLNL, April 5, 1983.

7. R. J. Briggs, J. C. Clark, T. J. Fessenden, R. E. Hester and E. J. Lauer, in Proceedings of the 2nd International Conference on High Power Electron and Ion Beam Research and Technology, (Cornell University, Ithaca, NY, 1977), Vol. I, p. 319.

8. Y. P. Chong, S. S. Yu, T. J. Fessenden, J. A. Masamitsu, A. M. Frank and D. S. Prono, "Spectral Measurements and Analysis of Beam Gas Emissions," LLNL UCRL-89679 (Preprint).

9. E. P. Lee, F. W. Chambers, L. L. Lodestro, and S. S. Yu, in Proceedings of the 2nd International Topical Conference on High Power Electron and Ion Beam Research and Technology, (Cornell University, Ithaca, NY, 1977), Vol. I, p. 381.

JCC:jma
6900v/ 0167v

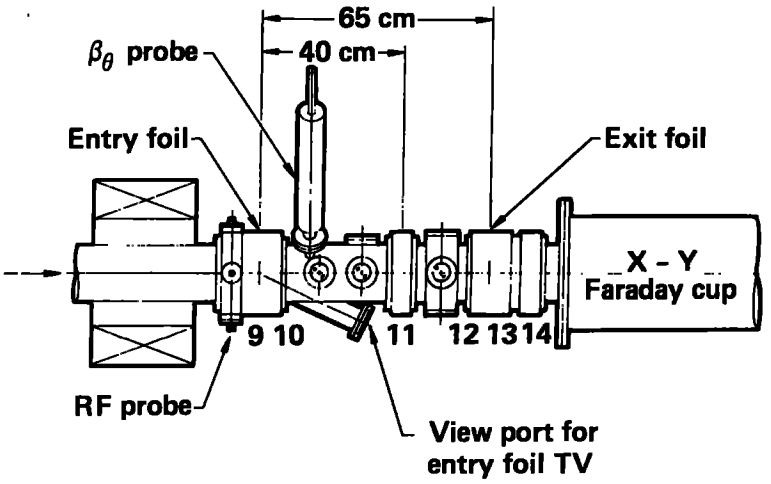
65 cm
40 cm
β_θ probe
Entry foil
Exit foil
X - Y
Faraday cup
9 10
11
12 13 14
RF probe
View port for
entry foil TV

Figure 1

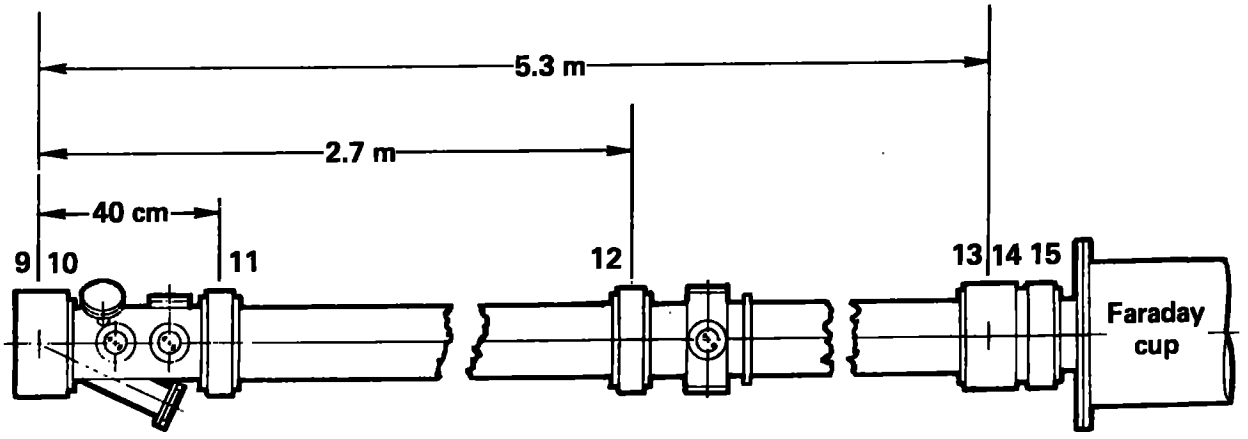

Figure 2

(a) Expanded cross section at microwave port

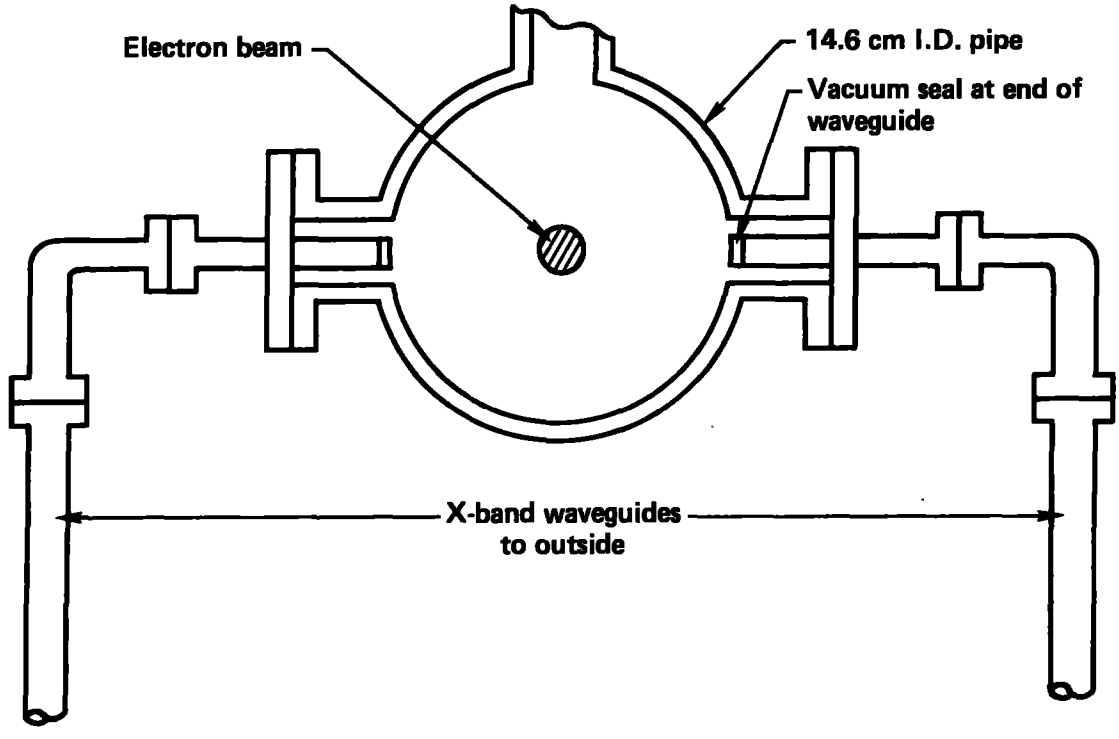

(b) Microwave detection outside shield

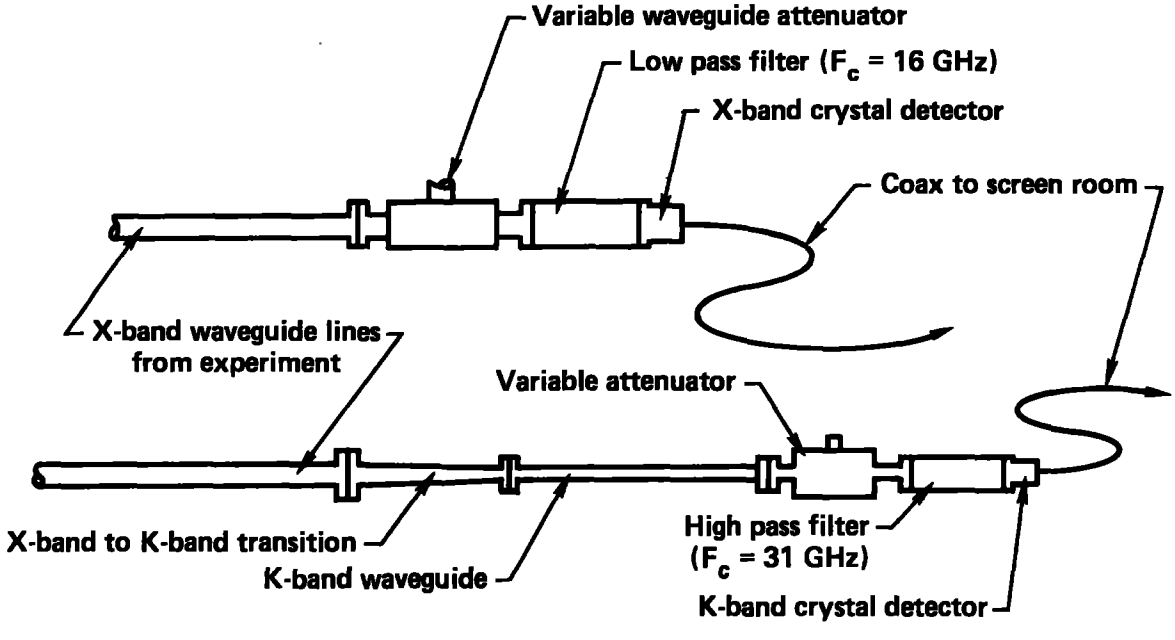

Figure 3

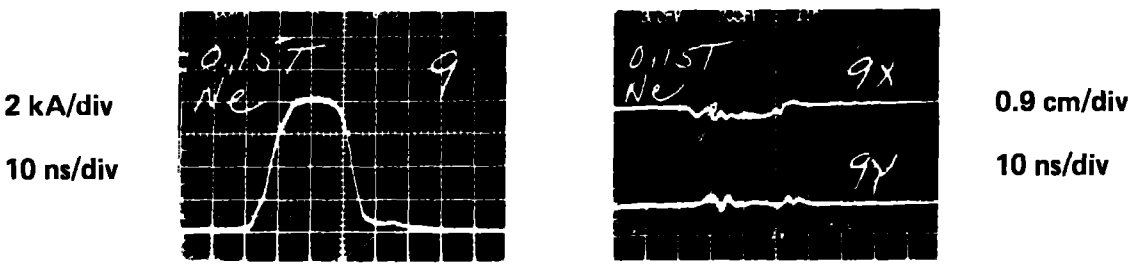

(a) (b)

Figure 4

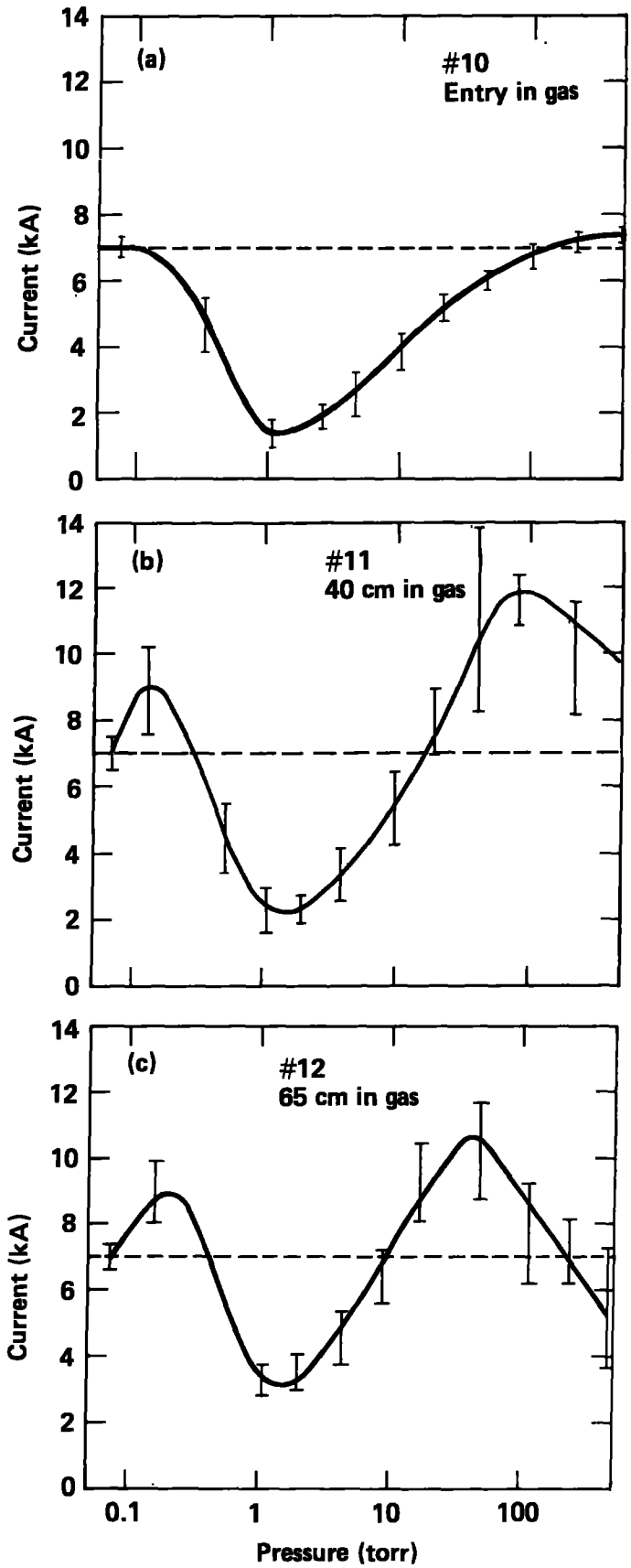
(a)
#10
Entry in gas
(b)
#11
40 cm in gas
(c)
#12
65 cm in gas
Current (kA)
Pressure (torr)
0.1
1
10
100
0
2
4
6
8
10
12
14

Figure 5

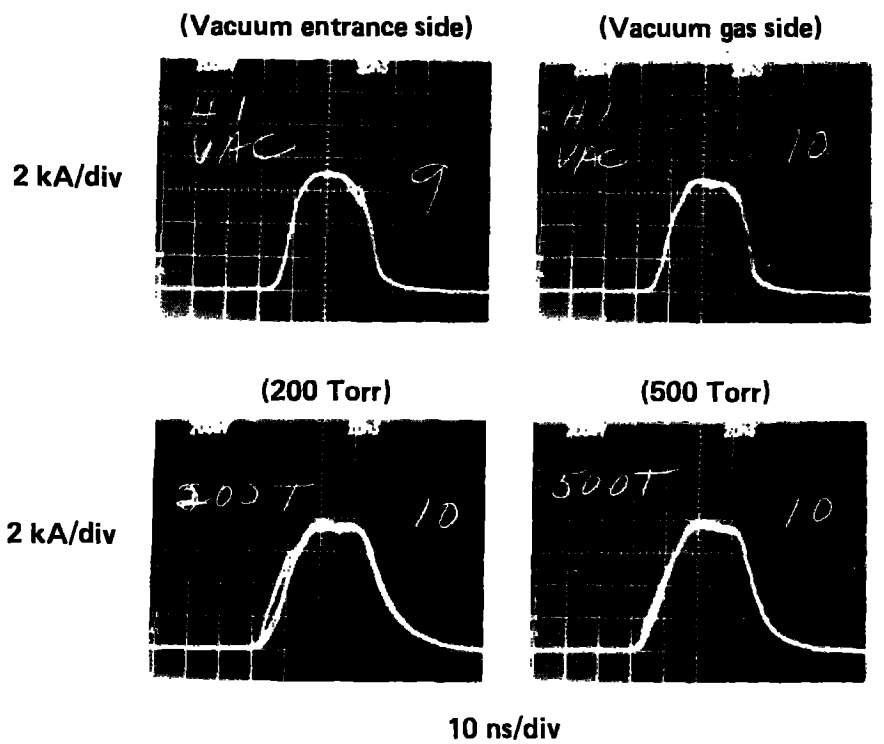
(Vacuum entrance side)
(Vacuum gas side)
2 kA/div
(200 Torr)
(500 Torr)
2 kA/div
10 ns/div

Figure 6

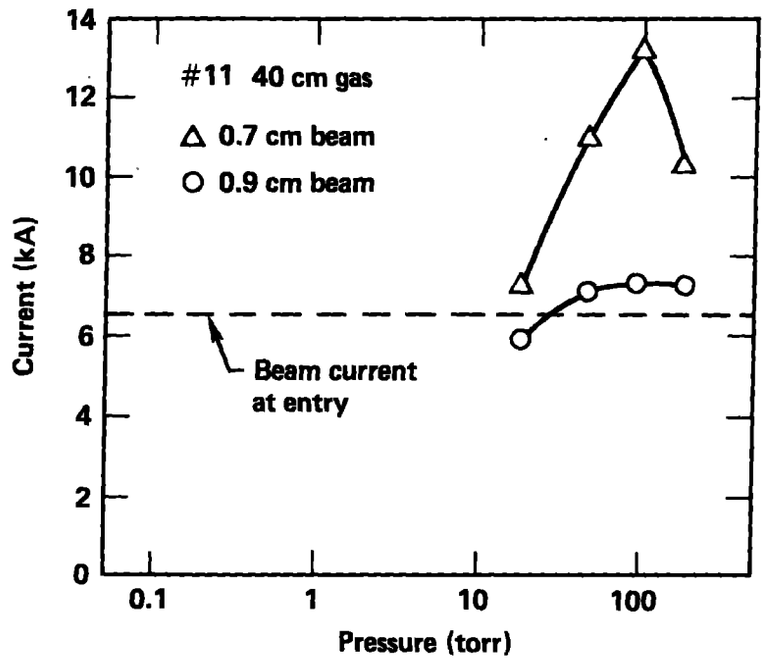
#11 40 cm gas
△ 0.7 cm beam
○ 0.9 cm beam
Beam current
at entry
Current (kA)
Pressure (torr)
0
2
4
6
8
10
12
14
0.1
1
10
100

Figure 7

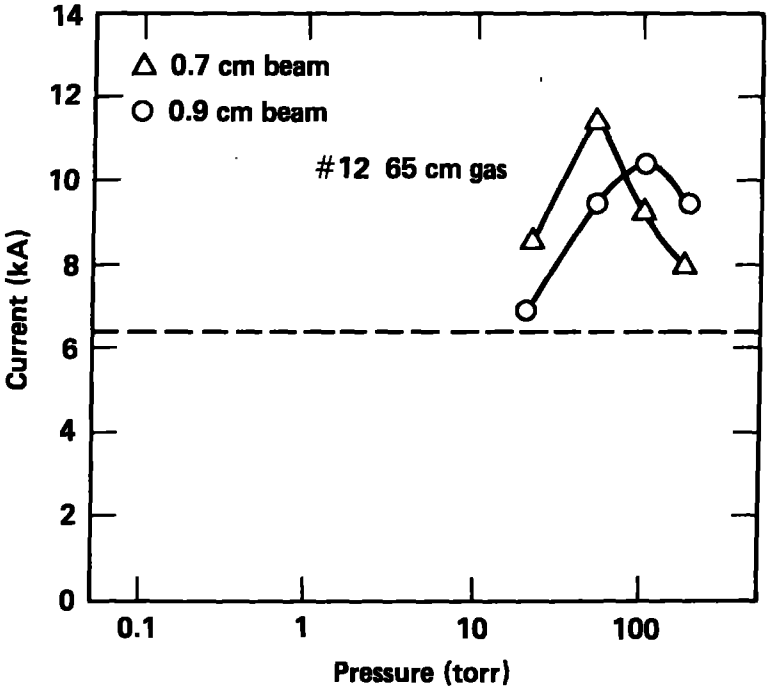
14
12
10
8
6
4
2
0
Current (kA)
△ 0.7 cm beam
○ 0.9 cm beam
#12 65 cm gas
0.1
1
10
100
Pressure (torr)

Figure 8

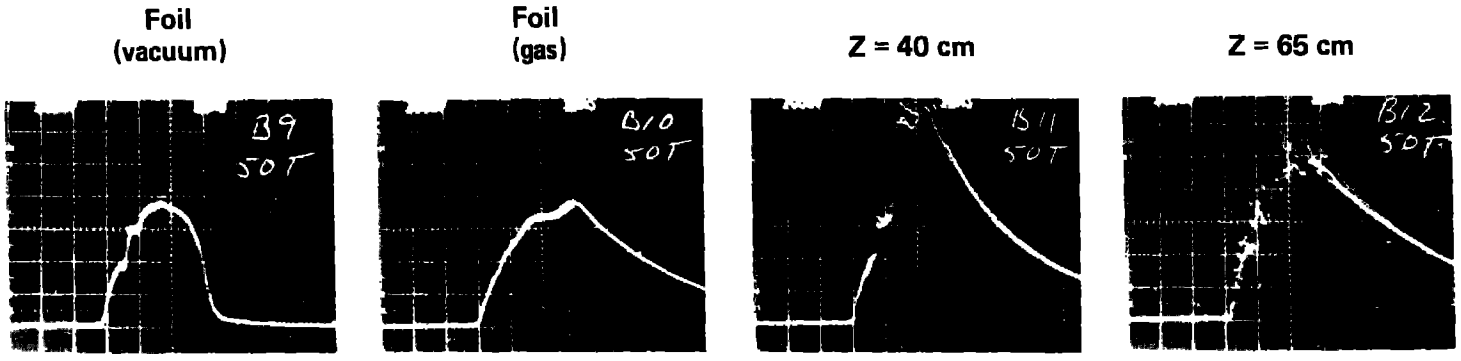
Foil
(vacuum)
Foil
(gas)
Z = 40 cm
Z = 65 cm
B9
50T
B10
50T
B11
50T
B12
50T
2 kA/div
10 ns/div

Figure 9.

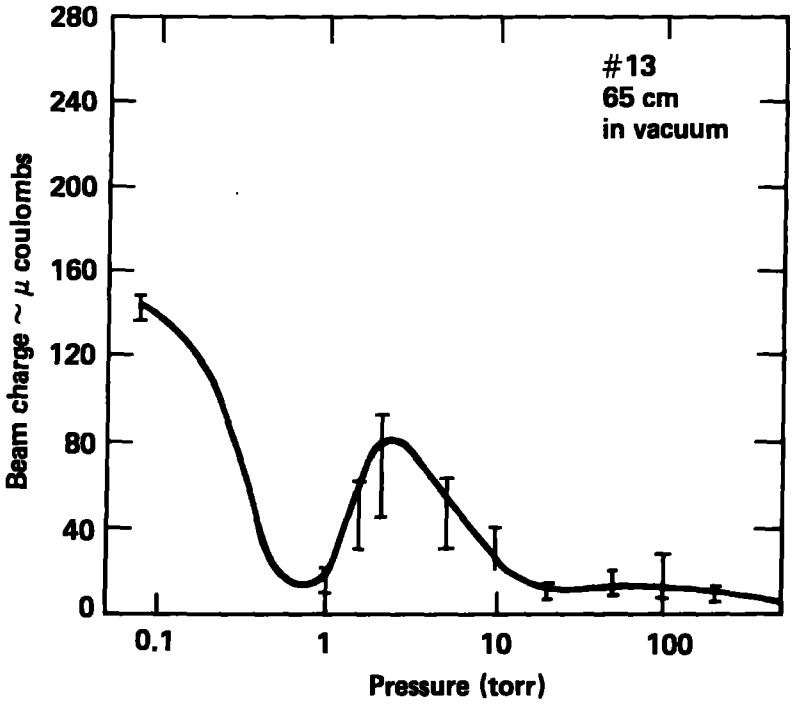
280
240
200
160
120
80
40
0
Beam charge ~ μ coulombs
#13
65 cm
in vacuum
0.1
1
10
100
Pressure (torr)

Figure 10

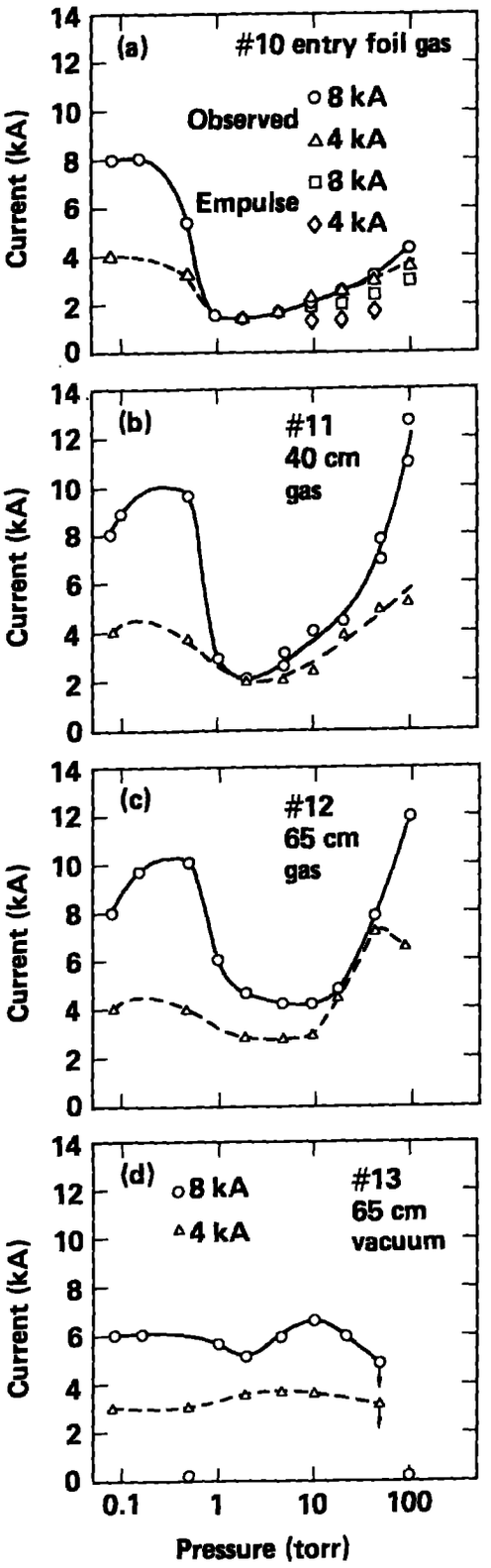
(a)
#10 entry foil gas
Observed
8 kA
4 kA
Empulse
8 kA
4 kA
(b)
#11
40 cm
gas
(c)
#12
65 cm
gas
(d)
8 kA
4 kA
#13
65 cm
vacuum
Current (kA)
Pressure (torr)
0.1
1
10
100

Figure 11

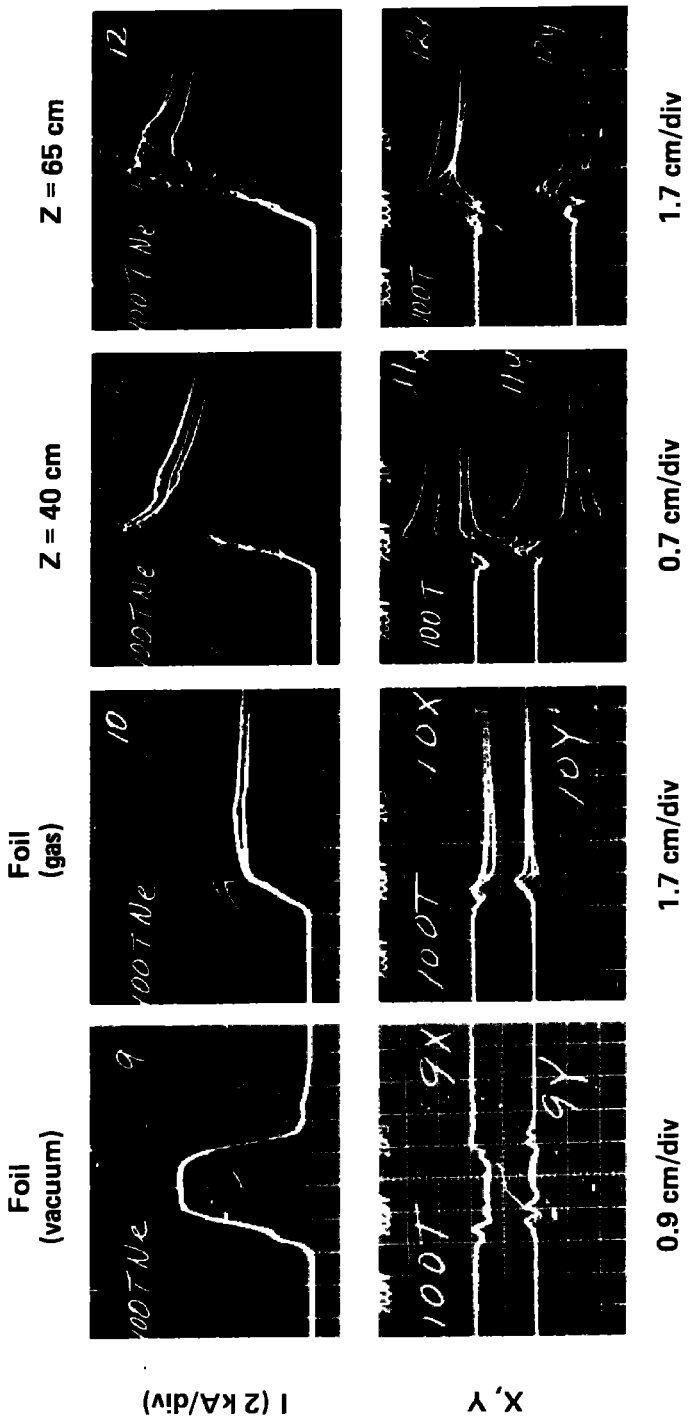
Foil (vacuum)
Foil (gas)
Z = 40 cm
Z = 65 cm
I (2 kA/div)
X, Y
0.9 cm/div
1.7 cm/div
0.7 cm/div
1.7 cm/div

Figure 12

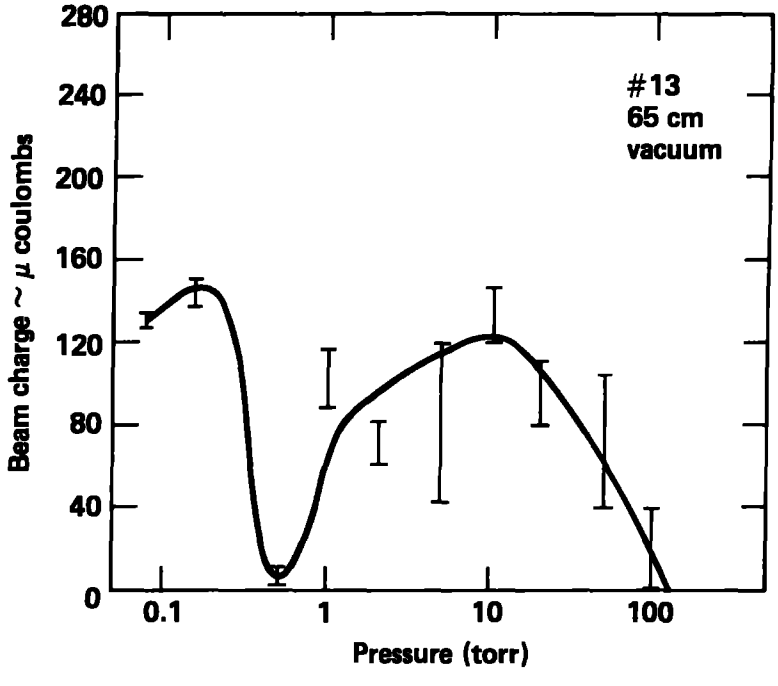
280
240
200
160
120
80
40
0
Beam charge ~ μ coulombs
#13
65 cm
vacuum
0.1
1
10
100
Pressure (torr)

Figure 13

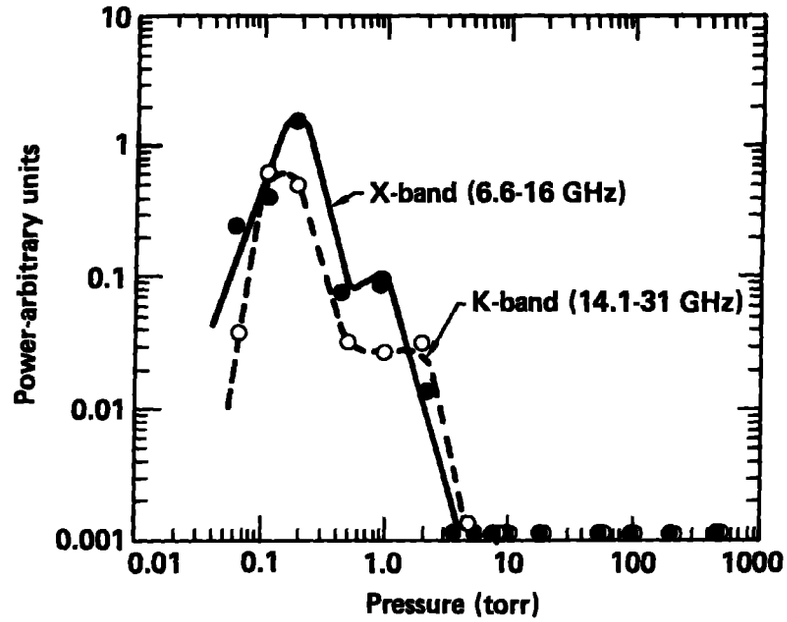
10
1
0.1
0.01
0.001
Power-arbitrary units
X-band (6.6-16 GHz)
K-band (14.1-31 GHz)
0.01
0.1
1.0
10
100
1000
Pressure (torr)

Figure 14

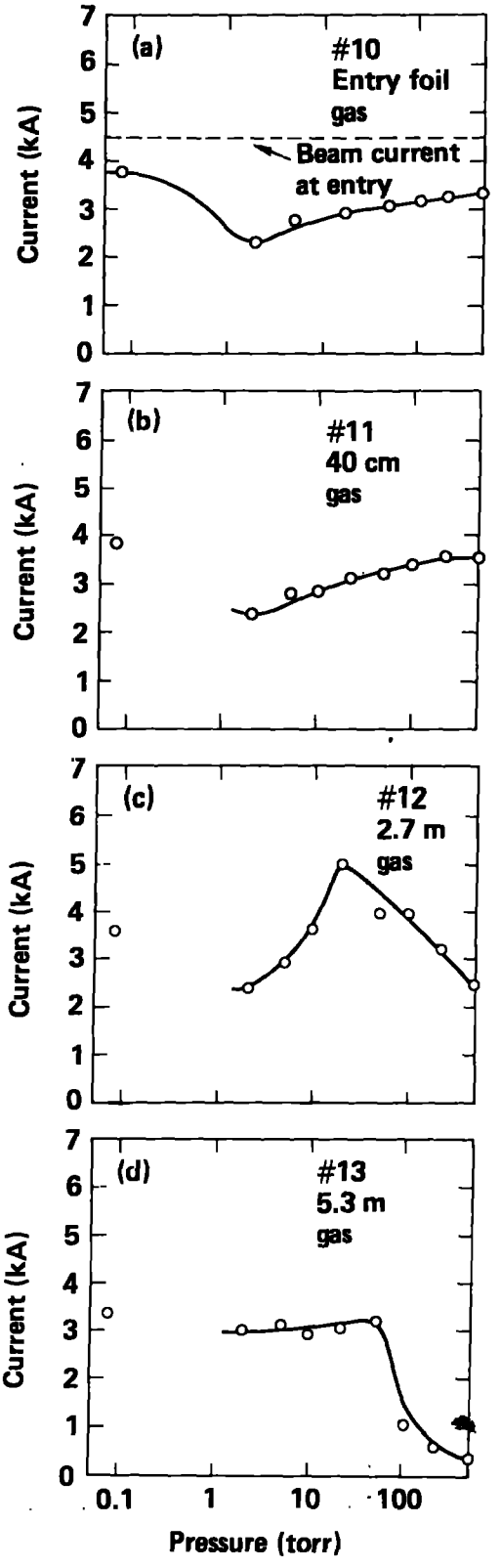
(a)
#10
Entry foil
gas
Beam current
at entry
(b)
#11
40 cm
gas
(c)
#12
2.7 m
gas
(d)
#13
5.3 m
gas
Current (kA)
0
1
2
3
4
5
6
7
0.1
1
10
100
Pressure (torr)

Figure 15

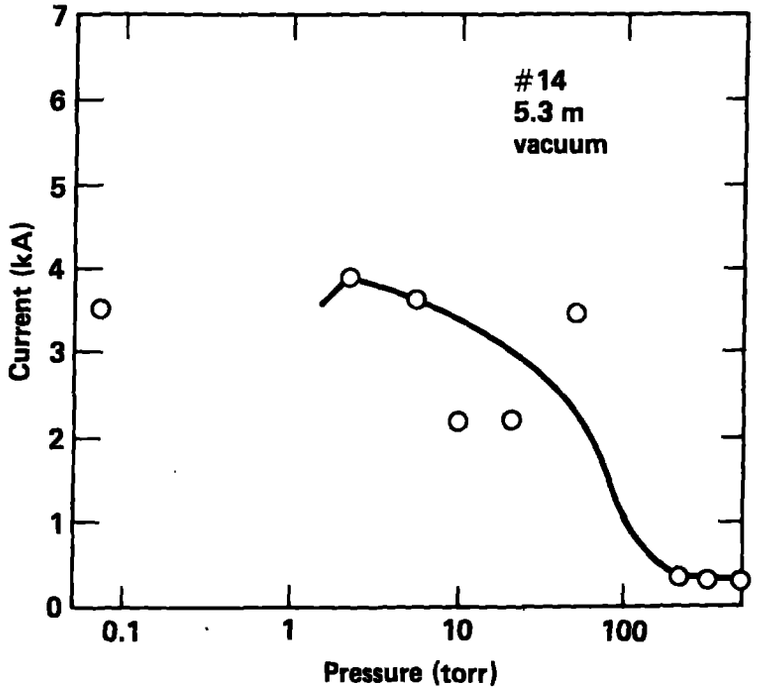

Figure 16

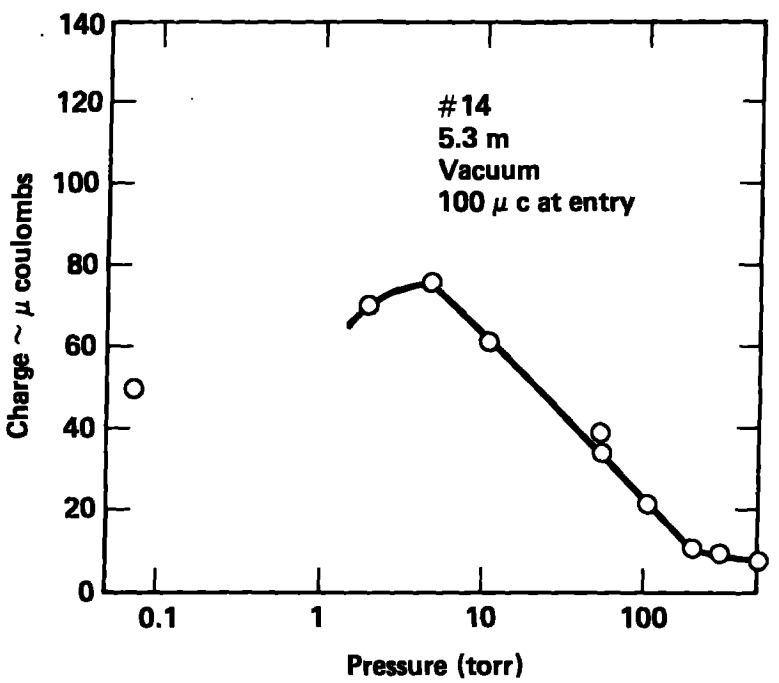
#14
5.3 m
Vacuum
100 μ c at entry
Charge ~ μ coulombs
140
120
100
80
60
40
20
0
0.1
1
10
100
Pressure (torr)

Figure 17

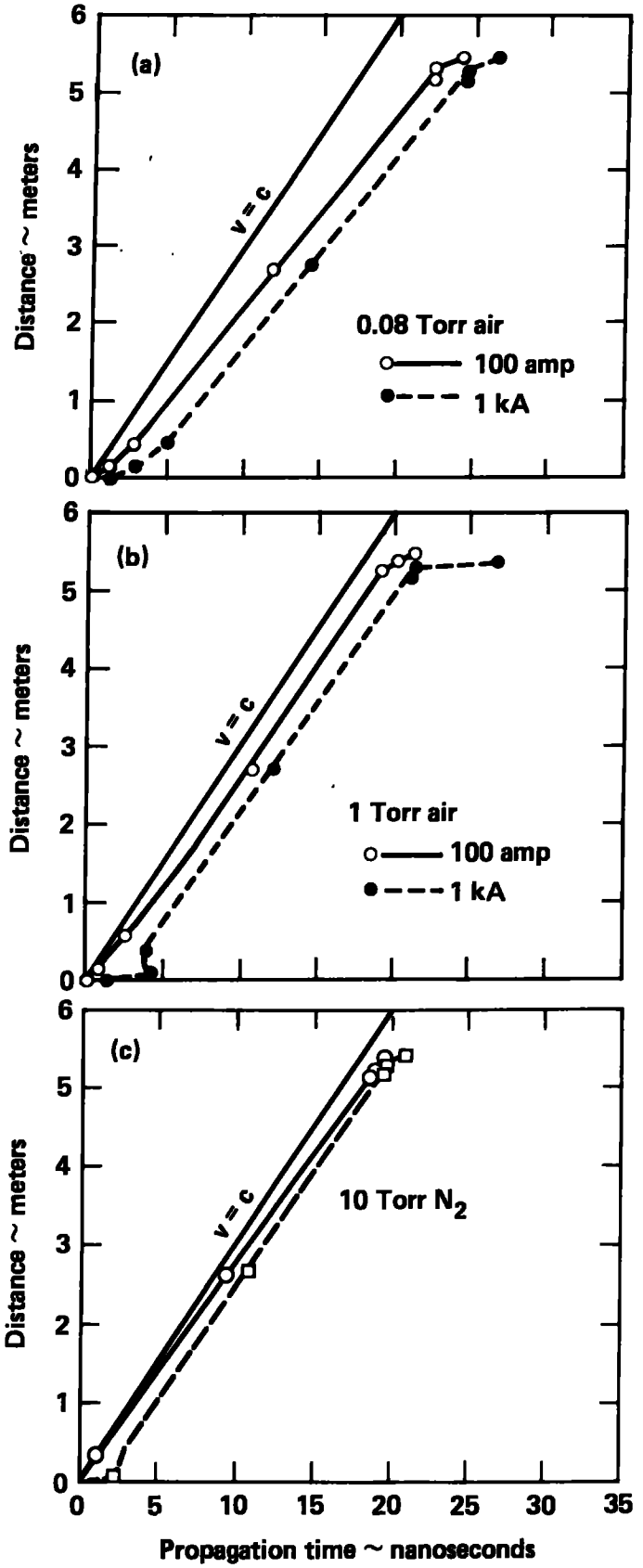
(a)
v=c
0.08 Torr air
100 amp
1 kA
(b)
v=c
1 Torr air
100 amp
1 kA
(c)
v=c
10 Torr N_2
Distance ~ meters
Propagation time ~ nanoseconds
0
1
2
3
4
5
6
0
5
10
15
20
25
30
35

Figure 18

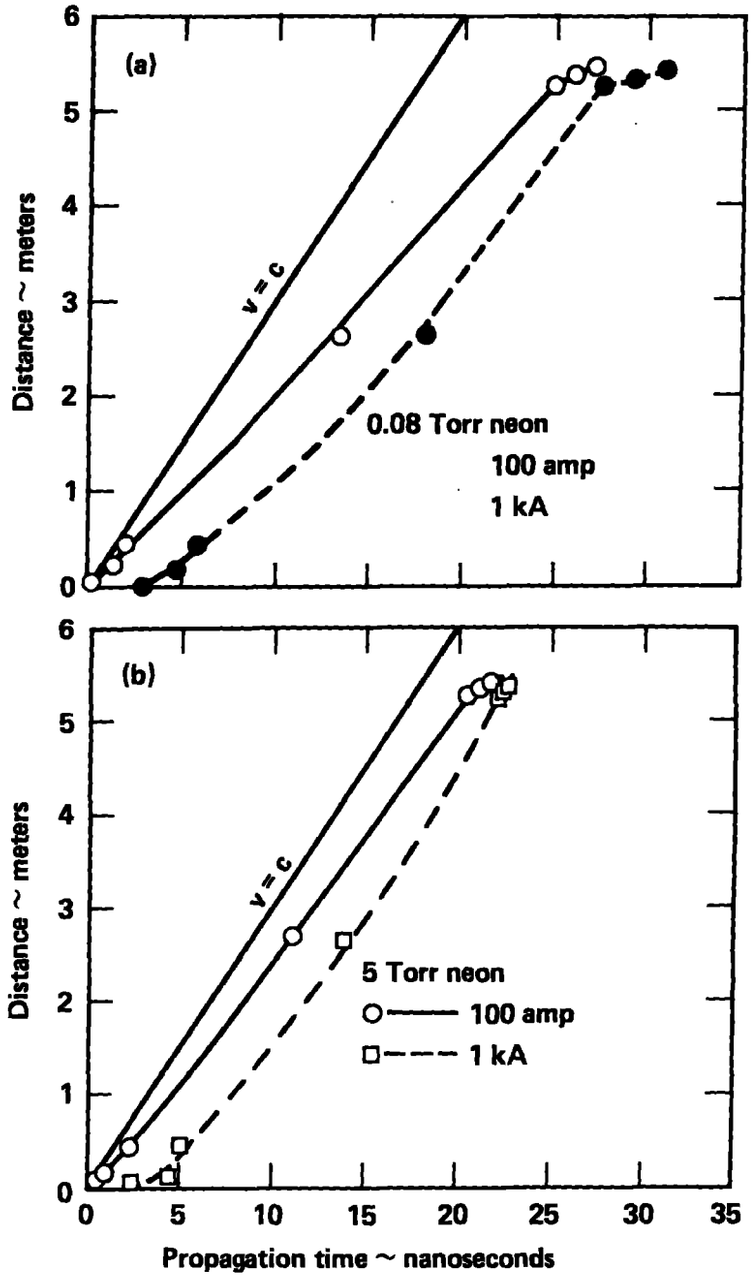
(a)
v=c
0.08 Torr neon
100 amp
1 kA
(b)
v=c
5 Torr neon
100 amp
1 kA
Distance ~ meters
Distance ~ meters
Propagation time ~ nanoseconds
0
1
2
3
4
5
6
0
5
10
15
20
25
30
35

Figure 19